COMPARATIVE ANALYSIS OF THE EXTENDED LIFTING-LINE THEORY TO THE CLASSICAL LIFTING-LINE THEORY FOR FINITE WINGS

Willian Mota Baldoino
Departamento de Engenharia Mecânica – DE-4
Instituto Militar de Engenharia (IME)
Praça General Tibúrcio, Nr 80 - Praia Vermelha
22290-270B Rio de Janeiro, RJ - Brasil
correio eletrônico: willian@ime.eb.br

Gustavo C.R. Bodstein
Departamento de Engenharia Mecânica – EE/COPPE, Universidade Federal do Rio de Janeiro
Centro de Tecnologia, Bloco G, sala 204 – Ilha do Fundão
21945-970 Rio de Janeiro, RJ – Brasil
correio eletrônico: gustavo@serv.com.ufrj.br

Abstract.. *Analytical and numerical comparisons are established between the extended and classical versions of the lifting-line theory in terms of aerodynamic performance parameters for an inviscid and incompressible flow over a finite wing with straight planform. Although classical lifting-line theory forms the foundation for preliminary aerodynamic design and also provides clear understanding of the wing theory, this paper shows that simulations of finite wings using the extended lifting-line theory can be carried out with relatively larger accuracy and without loss of the advantages provided by the classical lifting-line theory. The extended lifting-line theory also allows more flexibility in terms of the wing configurations that can be analyzed, including lower aspect ratios, swept lines and drifts, without increasing computational effort. In order to build the extended model the wing is divided into straight wing elements, each modeled by a horseshoe vortex with control points located at the three-quarter-chord line and with the bound vortex located at the one-quarter-chord line. Circulation distribution is then obtained for the control points by solving a set of linear algebraic equations based on an integral equation which expresses a statement of the no-penetration boundary condition applied to the local mean camber lines, spread spanwise. The circulation distribution, lift and induced drag coefficients and pitching moment coefficient are the aerodynamic parameters used for the comparison.*

Keywords: *classical lifting-line theory, extended lifting-line theory, aerodynamic parameters, aerodynamic performance.*

1. Introduction

It is very well known that Prandtl´s classical and extended lifting line theories form the foundation for aerodynamic design since they provide the conceptual basis for understanding finite wing theory and flight principles. Although lifting surface theory is still used to perform calculations with high accuracy, one must recognize that both lifting-line theories can be used for rapid estimation of finite wing performance parameters as well as spanwise load distribution of straight planform wings. Both lifting-line theories are formulated in terms of easy-handling integral equations. Many methods are available to deal with the classical lifting-line equation, which can be found in the books by Bisplinghoff et all. (1955), Robinson and Laurmann (1956), Thwaites (1960) and Schlichting and Truckenbrodt (1979). The most popular schemes for solving such equation are the collocation methods, which consist of assuming a finite sine series for the circulation distribution, and the Fourier series coefficients are determined by requiring the fundamental equation of Prandtl´s lifting-line theory to be identically satisfied at a number of spanwise locations from tip to tip. According to Rasmussen (1999) the major difficulty with the collocation methods is the lack of uniqueness and the arbitrary nature of the solution, since a given set of collocation points may describe more than one wing. Even so, if certain precautions are taken, like clustering the collocation points in such way that sudden changes are captured and enough terms and stations are assumed in order to presumably ensure adequate convergence, the scheme yields good results. Besides these arguments, the straightforwardness of this scheme entitles it to be used in the present comparative analysis.

Regarding the method for solving the equation of the extended lifting-line theory, a swept filament vortex is placed along the one-quarter-chord line and the induced velocity field, comprising self-induction and external induction, is then calculated at the three-quarter-chord line with the support of analytical tools such as Biot Savart Law and Helmholtz´s Vortex Theorems. The wing is divided into straight wing elements, each of them modeled by a horseshoe vortex with control points located at the three-quarter-chord line and with the middle point of the bound vortex located on the one-quarter-chord line, without loss of generality. The basic concept is to compute the strengths of each of the bound vortices required to keep the flow tangent to the wing surface at a set of control points. Extended lifting-line theory, also known as Weissinger Theory, differs from the classical lifting-line theory in several aspects, and it can be conceived as a simple panel method (a vortex lattice method with only one chordwise panel), as opposed to a corrected strip theory method, as the classical model is. The extended model works well with swept wings and, according to Glauert (1959), converges to the correct solution in both the high ad low aspect ratio limits. Another feature that causes the extended model to differ from the classical one is the fact that the non-uniqueness of the solution is dealt with using the Pistoles´s Theorem and Multropp´s methodl (Schlichting and Truckenbrodt, 1979), which allow the three-quarter-chord points of local stations to be assigned as the control points. As a consequence, the solution convergence depends essentially on

the size of the spanwise grid. These introductory ideas point out the advantage and limitations of each model and the numerical simulations shown below will highlight these differences.

2. Mathematical Formulation and Numerical Approach for the Classical Model

The fundamental equation of Prandtl´ s Lifting Line Theory is given by the following integro-differential equation

$$\alpha(y_o) = \frac{\Gamma(y_o)}{\pi U_{oo}\, c(y_o)} + \alpha_{L=0}(y_o) + \frac{1}{4\pi U_{oo}} \int_{-s}^{s} \frac{d\Gamma}{dy} \frac{dy}{y_o - y} \tag{1}$$

where α is the geometric angle of attack with respect to the zero lift line, $\alpha_{L=0}$ is the angle of zero lift, U_∞ is the freestream velocity, c is the local chord, Γ is the circulation distribution, $\pm s$ is the wing semi-span ($s = b/2$), y_o and y are the spanwise stations. Equation (1) states that the angle of attack is equal to the sum of the effective angle of attack, which is the angle actually seen by the local airfoil, and the induced angle of attack (last term). In terms of the following dimensionless variables

$$\eta = \frac{y_o}{s} \qquad \gamma = \frac{\Gamma}{U_{oo} b} \qquad c^* = \frac{c}{s} \tag{2}$$

the fundamental equation can be written as

$$\alpha(\eta) = \frac{2\gamma(\eta)}{\pi c^*(\eta)} + \alpha_{L=0}(\eta) + \frac{1}{2\pi} \int_{-1}^{1} \frac{d\gamma}{dn'} \frac{d\eta'}{\eta - \eta'} \tag{3}$$

The dimensionless form given by Eq.(3) is used to establish the analogy with the formulation of the extended model described below. Let us consider the transformation $y = -s\cos\theta$, where θ is the transforming coordinate in the spanwise direction. In terms of θ, the elliptical circulation distribution is written as $\Gamma(\theta) = -\Gamma_o \operatorname{sen}\theta$, where Γ_o is the circulation at the wing root. This suggests that a finite Fourier sine series is a suitable expression for the general circulation distribution. Hence, for the general case, the following expression is assumed

$$\Gamma(\theta) = 2bU_\infty \sum_{n=1}^{N} A_n \sin(n\theta) \tag{4}$$

Note that Eq. (4) satisfies the Kutta condition at the wing tips, which states that the upper and lower pressure fields must be equal at wing tips and, therefore, the circulation must be zero there. The substitution of Eq. (4) into Eq. (1), as described by Anderson (1991), yields

$$\alpha(\theta_o) = \frac{4}{\pi c^*(\theta)} \sum_{n=1}^{N} A_n \sin(n\theta_o) + \alpha_{L=0}(\theta_o) + \sum_{n=1}^{N} n A_n \frac{\sin(n\theta_o)}{\sin\theta_o} \tag{5}$$

Equation (5) is evaluated at a given spanwise station θ_o, where b, $c(\theta_o)$ and $\alpha_{L=0}$ are known quantities, and the only unknowns are the A_n's. If Eq. (5) is written for N different spanwise stations a system of N independent algebraic equations is obtained for the A_n's which satisfy the fundamental equation of finite-wing theory. This is the most straightforward scheme for solving the lifting-line equation, as described by Anderson (1991) and Rasmussen (1999). This solution is essentially a collocation method, whose main consequence is that, if sudden changes or any meaningful information in wing characteristics are to be captured, the points must be properly clustered. From Karamchetti (1966), it can also be seen that Eq. (4) results from the formulation for the flow in the Trefftz Plane (a plane far downstream from the wing) by using the method of the complex variable, so that the flow is solved in terms of a pair of analytic complex functions, that is, the complex potential and the associated complex velocity. Therefore, it is advisable conceiving Eq. (4) as the result of a classical method rather than a hint suggested by the coordinate transformation.

3. Mathematical Formulation and Numerical Approach for the Extended Model

The extended Lifting-Line Theory, or Weissinger Theory, can be conceived as a simple panel method, that is, a vortex lattice method with only one chordwise panel. However, it is not a corrected strip theory method, as the Classical

Lifting-Line Theory is. The extended model works for swept back or forwarded one-quarter-chord line wings, and also for wings with drift with respect to the freestream. This model converges to the correct solution in both the high and low aspect ratio limits. Essentially, the method is based on a discrete skewed horseshoe vortices, each of them consisting of a bound vortex and two trailing vortices extending to the infinite and a starting vortex located far downstream, so that this arrangement automatically satisfies the Helmontz requirement that no vortex line ends in the flow.

The basic concept is to compute the strengths $\Gamma_1, \Gamma_2,\ldots\Gamma_N$, of each bound vortices in order to keep the flow tangent to the wing surface at a set of control points. The arrangement comprising the relevant geometric features is depicted in Fig. (1), where the pair (ξ,η), $\xi = x/s$ denotes the dimensionless coordinate system and $\Gamma_1, \Gamma_2,\ldots\Gamma_N$ denote the strengths of the bound vortices placed along the one-quarter chord line.

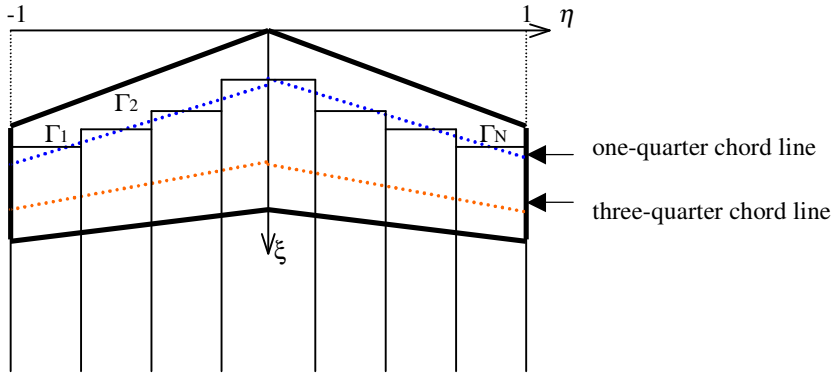

Figure 1. Discrete skewed horseshoe vortices on a finite wing for the extended model.

The kinematical no-penetration boundary condition applied to the local mean camber line of a given wing section is shown in Fig. (2), where α_g is the geometrical angle of attack, dz/dx is the mean camber line slope, and α is the angle of attack with respect to the zero lift line. Actually, α is an incidence angle that varies along the chordwise direction and it can be related to the geometrical angles.

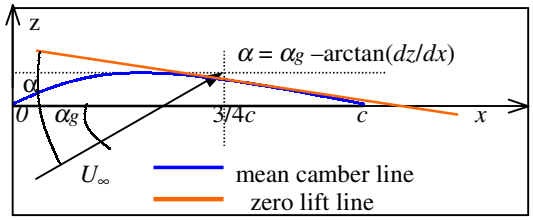

Figure 2. Geometric scheme of a local wing section at a given spanwise station.

3.1. Mathematical formulation

Unlike the simplicity of the Classical Lifting-Line Theory, derived in detail by Anderson (1991) with an interesting historical perspective, the Extended Lifting-Line Theory requires a little effort to gather essential concepts and formulae that lead to the assemblage of a concise mathematical model. The model is based on the assumptions that the flow over a finite wing is incompressible and irrotational, the approximations of thin local wing sections (thin airfoil theory) is valid, the angle of attack is small, and the aspect ratio is sufficiently high with respect to the chordwise direction, that is, $c/z_{max} >> 1$, where z_{max} is the maximum value of the camber.

The velocity field $\boldsymbol{U}$ is given by

$$\boldsymbol{U} = \boldsymbol{U}_\infty + \boldsymbol{w} \tag{6}$$

where $\boldsymbol{U}_\infty$ is the free stream velocity and $\boldsymbol{w}$ is the induced field due to the vortex system shown in Fig. (1). Boldface format indicates vector quantities. The use the approximations above allow the no-penetration boundary condition, $\boldsymbol{U} \cdot \boldsymbol{n} = 0$, to be transferred from the wing surface to the "camber" surface, where $\boldsymbol{n}$ is the outward unit vector on the mean camber line. By taking the above approximations into account, the linearized boundary condition can be written as

$$U_\infty\left(\alpha_g - \frac{dz}{dx}(x,z)\Big|_{x=3/4c}\right) + w(x,z) = 0 \tag{7}$$

A remarkable feature to be pointed out is that the incidence angle varies along the chordwise direction and this leads to the need for a criterion to define an adequate chordwise station to calculate the induced field w(x,z). In this respect, Pistolese ´ s theorem, based on the results from the thin airfoil theory, gives a powerful contribution, since it states that the calculation performed at the ¾ *c* point makes the incidence angle equal to the angle of attack with respect to the zero lift-line, that is, $\alpha = \alpha_g - \alpha_{L=0}$. As a result, the induced velocity field $w(x,z)$ due to the horseshoe vortex system distributed along the one-quarter chord line is calculated at the points located on the three-quarter chord line (control points). This is the reason for the extended model being known as the three-quarter-chord line method.

In the present context, the induced velocity field w(x,z) at a given point located on the three quarter chord line arise from the contributions of the trailing vortex system. It can be calculated by applying the Bio-Savart Law to each of the semi-infinite vortex filaments, computing the induced velocity due to the legs that bounds the point (self-induction or downwash component) and the induced velocity due to the external legs (external induction or upwash component). The additional assumptions for the extended model are: the circulation per unit length is constant along each horseshoe vortex and the control point is placed, without loss of generality, at the midpoint of the horseshoe vortex. This arrangement is shown in Fig. (3), where yhe pair (x_p,y) denotes the control point coordinates, (x_c,y') denotes the bound vortex coordinates (left leg), $\varepsilon = dy$ is the grid step; $\xi_p = x_p/s$, $\xi_c = x_c/s$, $\eta' = y'/s$ and $\eta = y/s$ are the dimensionless coordinates used in the Weissinger method.

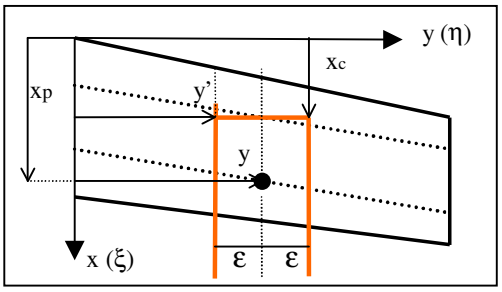

(a) Self-induction contribution–downwash component;

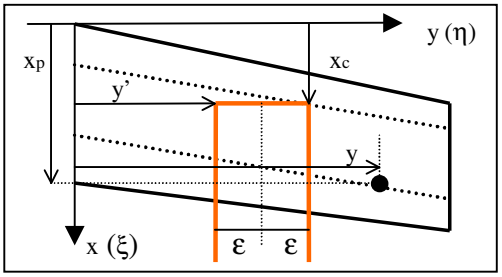

(b) External induction contribution – upwash component;

Figure 3. Horseshoe vortex contributions to induced velocity at the three-quarter-chord point.

Because a detailed derivation of the induced velocity can be found in Schilchting and Truckenbrodt (1979), only the main results obtained from Biot-Savart Law is presented here. The Induced velocity field *w* is split into the downwash w_d and the upwash w_u components as follows. The downwash *wd* component and upwash component *wu* at an arbitrary control point are respectively given by

$$w_d = -\frac{\Gamma(y)}{\pi\varepsilon},\ \varepsilon \to 0 \tag{8}$$

$$w_u = \int_{-s}^{s} \frac{\Gamma(y')\,dy}{4\pi(y-y')^2}\left[1 + \frac{x_P(y) - x_c(y')}{\sqrt{(x_P(y) - x_c(y'))^2 + (y-y')^2}}\right] \tag{9}$$

The integration is performed with respect to y' throu gh the interval $-b/2 \le y' \le b/2$ where y must be excluded .The integral represents the contribution of the vortex system to the induced velocity at $y' = y_p$, where a singularity takes place. Substitution of Eq. (8) and Eq. (9) into Eq. (7) and the use of Pistolese's theorem $\alpha = \alpha_g$ –arctan (dz/dx) at $x = x_p$, yields the following integro-differential equation for the circulation distribution $\Gamma(y)$

$$U_\infty \alpha(y) = \frac{1}{4\pi} \lim_{\varepsilon \to 0} \left[\frac{4\Gamma(y)}{\varepsilon} - \int_{-s}^{s} \frac{\Gamma(y')}{(y-y')^2} \left(1 + \frac{x_p(y) - x_c(y')}{\sqrt{(x_p(y) - x_c(y'))^2 + (y-y')^2}} \right) dy' \right] \tag{10}$$

Defining the function $G(x_p, y; y')$ as

$$G(x_p, y; y') = \Gamma(y') \left(1 + \frac{x_p(y) - x_c(y')}{\sqrt{(x_p(y) - x_c(y'))^2 + (y-y')^2}} \right) \tag{11}$$

Equation (10) can be rewritten as

$$U_\infty \alpha(y) = \frac{1}{4\pi} \lim_{\varepsilon \to 0} \left[\frac{4\Gamma(y)}{\varepsilon} - \int_{-s}^{s} \frac{G(y')}{(y-y')^2} dy' \right] \quad ; \quad G(x_p, y; y') = 2\Gamma(y) \quad \text{at} \quad y = y' \tag{12}$$

Due to the singularity at $y' = y$ the integration domain must be split into two intervals $[-s, y-\varepsilon) \cup (y+\varepsilon, s]$. A first analogy can be established, in analytical terms, between the classical and extended models using the dimensionless form of Eq. (10) as follows

$$\alpha(\eta) = \frac{1}{4\pi} \lim_{\varepsilon^* \to 0} \left[\frac{4\gamma(\eta)}{\varepsilon^*} - \int_{-1}^{1} \frac{F(\xi_p, \eta; \eta')\gamma(\eta')}{(\eta - \eta')^2} d\eta' \right] \tag{13}$$

$$\gamma(\eta) = \frac{\Gamma(y)}{bU_\infty} \qquad F(\xi_p, \eta, \eta') = 1 + \frac{\xi_p(\eta) - \xi_c(\eta')}{\sqrt{(\xi_p(\eta) - \xi_c(\eta'))^2 + (\eta - \eta')^2}} \qquad \varepsilon^* = \frac{\varepsilon}{s} \tag{14}$$

After some algebraic manipulation the extended model equation becomes

$$\alpha(\eta) = \lim_{\varepsilon^* \to 0} \left[\frac{2\gamma(\eta)}{\pi\varepsilon^*} - \frac{1}{\pi} \int_{-1}^{1} \frac{\gamma(\eta')}{(\eta - \eta')^2} d\eta' \right] + \frac{1}{2\pi} \int_{-1}^{1} K(\xi_P, \eta, \eta')\gamma(\eta') d\eta' \tag{15}$$

where

$$K(\xi_P, \eta; \eta) = \frac{2 - F(\xi_P, \eta, \eta')}{(\eta - n')^2} \tag{16}$$

For the sake of comparison, Eq. (3) is rewritten here

$$\alpha(\eta) = \frac{1}{2\pi} \int_{-1}^{1} \frac{d\gamma}{dn'} \frac{d\eta'}{\eta - \eta'} + \frac{2\gamma(\eta)}{\pi c^*(\eta)} + \alpha_{L=0} \tag{17}$$

Comparing Eq. (15) and Eq. (17), some remarkable similarities can be pointed out. The first one arises from the first term on the right-hand side of both equations since they represent the Cauchy Integral Formula, with a singularity at $\eta' = \eta$. Actually, the first term in Eq. (15) equals the induced angle of attack far downstream, and this result can also be shown by calculating Eq. (13) in the limit $x_p - x_c >> \max \, || y - y' || \approx b = 2s$ or $\xi_p - \xi_c >> 2$. It should be emphasized that this is a mathematical analogy rather than a physical one, because the induced angle of attack is calculated far away

from the wing. The second similarity arises from the fact that the second term on the right-hand side of both equations possesses an exclusive dependence on the wing planform geometric characteristics. Indeed, the function $K(\xi_p, \eta, \eta')$, defined in Eq. (16), is regular at $\eta' = \eta$ and this can be shown with the aid of the L' Hôspital's rule. A third similarity is that no reference has been made to Kutta condition at the wing tips, which represents an additional boundary condition to be taken into account by the method used to solve the integro-differential equations. For the classical model the finite Fourier sine series given by Eq. (4) is assumed to be a solution, which satisfies the Kutta condition. Regarding the extended model, further development from Eq. (13) is required. No matter how refined the grid scheme is, any attempt to solve Eq. (15) for velocity circulation does not work out because Kutta condition has not been imposed yet.

Further algebraic manipulations involving Eq.(13) and Eq.(15) provide other interesting insights. For example, an integration by parts involving the Cauchy integral in Eq. (15) furnishes meaningful information about the streamwise distribution of the downwash on the vortex sheet. Also, integration by parts involving the Cauchy integral in Eq. (13) yields a more suitable version for comparison purposes in terms of integro-differential equations, besides allowing the the Kutta condition to be satisfied. Starting with the first term in Eq. (15) :

$$\alpha_i^{\infty} = \lim_{\varepsilon^* \to 0}\left[\frac{2\gamma(\eta)}{\pi\varepsilon^*} - \frac{1}{\pi}\int_{-1}^{1}\frac{\gamma(\eta')}{(\eta-\eta')^2}d\eta'\right] = \lim_{\varepsilon \to 0}\left[\frac{\Gamma(y)}{\pi\varepsilon U_\infty} - \frac{1}{2\pi U_\infty}\int_{-s}^{s}\frac{\Gamma(y')}{(y-y')^2}dy'\right]$$

$$= \frac{\Gamma(y)}{\pi\varepsilon U_\infty} - \frac{1}{2\pi U_\infty}\left[\frac{\Gamma(y)}{y-y'}\bigg|_{-s}^{y-\varepsilon} + \frac{\Gamma(y)}{y-y'}\bigg|_{y+\varepsilon}^{s} - \int_{-s}^{s}\frac{\Gamma'(y')}{y-y'}dy'\right]$$

$$= \frac{\Gamma(y)}{\pi\varepsilon U_\infty} - \frac{1}{2\pi U_\infty}\left[\frac{\Gamma(y)}{y-y'}\bigg|_{-s}^{y-\varepsilon} + \frac{\Gamma(y)}{y-y'}\bigg|_{y+\varepsilon}^{s} - \int_{-s}^{s}\frac{\Gamma(y')}{y-y'}dy'\right] \tag{18}$$

$$\alpha_i^{\infty} = 2\alpha_i^{wing} = \frac{1}{2\pi U_\infty}\left[\int_{-s}^{s}\frac{\Gamma(y')}{y-y'}dy'\right] \tag{19}$$

where α_i^{∞} denotes the angle of attack far downstream and α_i^{wing} denotes the angle of attack at the wing station $y' = y$. The Kutta condition has been accounted for through the condition $\Gamma(s) = \Gamma(-s) = 0$, and also $\Gamma(y-\varepsilon) = \Gamma(y+\varepsilon) = \Gamma(y)$ when $\varepsilon \to 0$, which are automatically satisfied. It is clear from Eq. (19) that the induced angle α_i^{wing} is the same as the induced angle of attack for the Classical Lifting-Line Theory, as shown in Eq. (1). This result represents a powerful contribution to Trefftz's method. The reader is warned not to get confused by the superscripted circulation Γ' denoting first derivative with respect to y' .

Now, integrating the second term in Eq. (13) by parts gives

$$\int_{-1}^{1}\frac{F(\xi_p,\eta;\eta')\gamma(\eta')}{(\eta-\eta')^2}d\eta' = \frac{F(\xi_p,\eta;\eta')\gamma(\eta')}{\eta-\eta'}\bigg|_{-1}^{\eta-\varepsilon^*} + \frac{F(\xi_p,\eta;\eta')\gamma(\eta')}{\eta-\eta'}\bigg|_{\eta+\varepsilon^*}^{1}$$

$$-\int_{-1}^{1}\frac{F(\xi_p,\eta;\eta')\gamma'(\eta')}{(\eta-\eta')}d\eta' - \int_{-1}^{1}\frac{F'(\xi_p,\eta;\eta')\gamma(\eta')}{\eta-\eta'}d\eta' \tag{20}$$

Further development of Eq. (20) must include the Kutta condition $\gamma(-1) = \gamma(1) = 0$ and $F(\xi_p,\eta;\eta-\varepsilon^*) = F(\xi_p,\eta;\eta+\varepsilon^*) \to 2$; $\gamma(\eta-\varepsilon^*) = \gamma(\eta+\varepsilon^*) \to \gamma(\eta)$ as $\varepsilon^* \to 0$. Finally, the substitution of the result into Eq. (13) yields:

$$\alpha(\eta) = \frac{1}{2\pi}\lim_{\varepsilon^* \to 0}\left[\int_{-1}^{1}\frac{F(\xi_p,\eta;\eta')\gamma'(\eta')}{\eta-\eta'}d\eta' + \int_{-1}^{1}K^*(\xi_p,\eta;\eta')\gamma(\eta')d\eta'\right] \tag{21}$$

$$K^*(\xi_p,\eta;\eta') = \frac{F'(\xi_p,\eta;\eta')}{\eta-\eta'} = \frac{\xi_p(\eta)-\xi_c(\eta')}{\left[(\xi_p(\eta)-\xi_c(\eta'))^2 + (\eta-\eta')^2\right]^{3/2}} \tag{22}$$

Again, the superscripted quantities F' and γ' denote first derivative with respect to η'. Equation (21) represents an important analytical result, since it embodies both the kinematical boundary condition and Kutta condition. An analogy can also be established between Eq. (21) and Eq. (17). The first terms in both equations represent the Cauchy Integral Formulae as described by Karamchetti (1966) and they are essentially related to induced effects (induced angle of attack and induced velocity field) and the second terms are exclusive functions of the wing planform geometric characteristics. From Eq. (22) it can be easily seen that the function K^* is regular at $\eta' = \eta$. It is clear from the developments presented so far, even in analytical terms, that extended model reveals features on the finite wing theory otherwise unable to be seen through the classical one. Indeed, if one tries to retrieve the past, turning back to the beginning of the last century (Anderson, 1991), it is possible to see, in the scope of the lifting-line theory, labeled as Lanchester-Prandtl theory, that the finite wing was simply conceived as a straight vortex filament with a circulation that varies as a function of the spanwise coordinate y. On the on hand, it represented a huge step in aeronautical sciences at that time. On the other hand, it was just a tiny step in a series of theories that led to a set of powerful analytical tools available today. For historical reasons, the extended model has been developed in a dimensionless form to meet the definitions from the Weissinger coordinate system. However, in the present context, the numerical scheme used to solve the problem is based on the dimensional form of Eq. (22), which reads

$$\alpha(y) = \frac{1}{4\pi U_\infty}\int_{-s}^{s} \frac{F(x_p, y; y')\Gamma'(y')}{y - y'} dy' + \frac{1}{4\pi U_\infty}\int_{-s}^{s} \hat{K}(x_p, y; y')\Gamma(y')dy' \tag{23}$$

$$\hat{K}(x_p, y; y') = \frac{x_p(y) - x_c(y')}{\left[(x_p(y) - x_c(y'))^2 + (y - y')^2\right]^{3/2}} \tag{24}$$

$$F(x_p, y; y') = 1 + \frac{x_p(y) - x_c(y')}{\left[(x_p(y) - x_c(y'))^2 + (y - y')^2\right]^{1/2}} \tag{25}$$

3.2. Numerical formulation

Equation (23) is discretised according to scheme shown in Fig. (4).

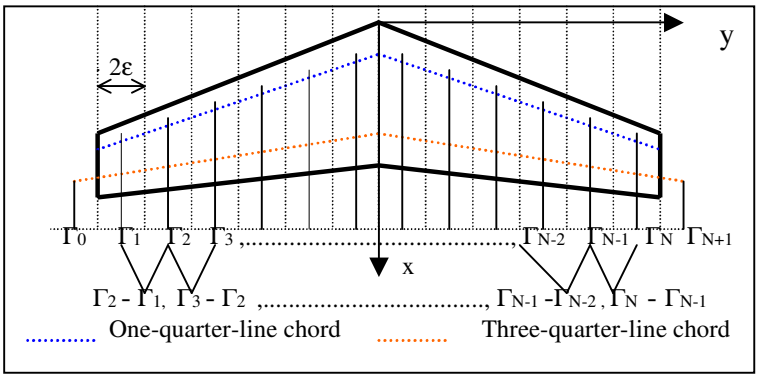

Figure 4. Numerical discretisation scheme for the extended model

The circulation is assumed constant through each of the horseshoe vortices, and $\Gamma_0 = \Gamma_{N+1} = 0$. As shown in Fig. (4), a control point is placed at the midpoint of each horseshoe vortex and a uniform grid is adopted. A high-order precision requires a large number of elemental rectangular wings ($N \to \infty$), which means $\varepsilon \to 0$. Since this proceedure is mostly concerned with the comparison between two mathematical models for a finite wing calculation, higher order approximations have not been considered. Actually, if the linear system of algebraic equations for the extended model is properly assembled, the numerical precision is not a concern. The space discretisation of the first term on the right-hand side of Eq. (23), according to geometrical scheme shown in Fig. (4), yields

$$1 \le i \le N \text{ and } \le j \le N \tag{26}$$

$$F(i,j)=1+\frac{x_p(i)-x_c(j)}{\sqrt{(x_p(i)-x_c(j))^2+(y(i)-y(j))^2}} \tag{27}$$

$$\Theta(i,1)=-\frac{F(i,1)}{i-1}+f(i);\ f(i)=\frac{F(i,0)}{i} \quad 2\le i\le N \tag{28}$$

$$\Theta(1,1)=f(1) \tag{29}$$

$$F(i,0)=1+\frac{x_p(i)-x_c(0)}{\sqrt{(x_p(i)-x_c(0))^2+(y(i)+s)^2}}\ ;\ x_c(0)=s\tan(\Lambda_{le})+\frac{c_t}{4} \tag{30}$$

$$\Theta(j.j)=F(j,j-1) \quad ;\ 2\le j\le N \tag{31}$$

$$\Theta(j,j+1)=F(j.j+1) \quad ;\ 1\le j\le N-1 \tag{32}$$

$$\Theta(i,j)=\frac{F(i,j-1)}{i-j+1}-\frac{F(i,j)}{i-j} \quad ;\ 1\le i\le N-2 \text{ and } i+2\le j\le N \tag{33}$$

$$\Theta(i,j)=\frac{F(i,j-1)}{i-j+1}-\frac{F(i,j)}{i-j} \quad ;\ 3\le i\le N \text{ and } 2\le j\le i-1 \tag{34}$$

where c_t is the tip chord, Λ_{le}, is the leading edge sweepback angle and $\Theta(i,j)$ is a matrix derived from the rearrangement of the difference scheme. This first discretisation is concerned with induced angle of attack at the i^{th}-spanwise station.

The space discretisation of the second term on right hand side of Eq. (23), according to geometrical scheme shown in Fig. (4), yields

$$\alpha_{ef}(i)=\frac{\varepsilon}{2\pi U_\infty}\sum_{j=1}^{N}\hat{K}(i,j)\Gamma(j) \tag{35}$$

$$\hat{K}(i,j)=\frac{x_p(i)-x_c(j)}{\left[(x_p(i)-x_c(j))^2+4\varepsilon^2(i-j)^2\right]^{3/2}} \tag{36}$$

where $\alpha_{ef}(i)$ denotes the "analogous" of the effective angle of attack at the i^{th}-spanwise station. Now, the space discretisation of the left hand side of Eq. (23) yields

$$\alpha(i)=\alpha_g(i)-\frac{dz}{dx}(x_p(i),z(i)) \tag{37}$$

where $\alpha_g(i)$ is the geometric angle of attack quoted at i^{th}-spanwise station of the discretised wing. For wings geometrically twisted, a linear twist model is usually assumed:

$$\alpha_g(i)=\alpha_{root}+\varphi\,|y(i)| \tag{38}$$

where α_{root} is the geometric angle of attack at the wing root and φ is the twist per unit length along the spanwise direction ($\varphi<0$ for washout distribution). A final consideration to get the circulation distribution is that the Weissinger theory provides the means for computing the distribution of lift on swept wings, but not the chordwise distribution of pressure. It is mostly for this reason that the Simple Sweep Theory must be embodied on the present formulation. The main idea behind sweeping the wing is to reduce the effects of compressibility. Although the compressibility is not a reason for concern in the present context, it cannot be denied that the component of the flow parallel to the wing is affected by the presence of the wing, so that the normal component is decoupled from the tangential component. As a result, the sections normal to leading edge can be considered as operating in the flow with lower velocity and dynamic pressure. From these considerations, the extended model incorporates a sweeping effect. The solution for the circulation distribution is simply obtained by solving $\alpha(i)=\alpha_g(i)+\alpha_{ef}(i)$, which yields the following system of linear algebraic equations.

$$A_{ij}\,\Gamma_j = B_i \qquad 1 \le i \le N \;\; ; \;\; 1 \le j \le N \tag{39}$$

$$A_{ij} = \frac{\Theta_{ij}}{4\varepsilon} + \varepsilon \hat{K}_{ij} \qquad B_i = 2\pi U_\infty \cos\Lambda_{1/4} \left(\alpha_{root} + \varphi |y_i| - \frac{dz}{dx}(x_p(i), z_i) \right) \tag{40}$$

where $\Lambda_{1/4}$ is the sweepback angle of the one-quarter-chord line with respect to axis y. Since the system of linear equations expressed in Eq. (38) meets the diagonal dominance requirement, it can be solved by means of implicit methods, like Gauss elimination. Once the circulation distribution is available, the inviscid wing parameters can be obtained through the following equations:

$$L'(y) = \rho U_\infty \Gamma(y) \;\; ; \;\; c_l(y) = \frac{2\Gamma(y)}{U_\infty c(y)} \;\; ; \;\; C_L = \frac{2}{U_\infty S}\int_{-s}^{s} \Gamma(y)\,dy \tag{41}$$

$$C_{Di} = \frac{2}{U_\infty S}\int_{-s}^{s} \Gamma'(y)\,\alpha_i(y)\,dy \quad ; \quad C_{my} = -\frac{2}{U_\infty S\, c}\int_{-s}^{s} \Gamma'(y)\; x^*(y)\,dy \tag{42}$$

where L' is the lift distribution (the superscript L' indicates lift per unit length), c_l is the local lift coefficient, C_L is the wing lift coefficient, C_{Di} is the wing induced drag coefficient, C_{my} is the wing pitching moment coefficient with respect to a line parallel to the y-axis passing through the one-quarter-chord point at wing root, that is, $x^*(y) = x(y) - c_r/4$ (c_r is the root chord), $c(y)$ is the local chord, S is the wing planform area and c is an average of $c(y)$. Unlike the classical model, the wing performance parameters such as the induced drag factor and the span efficiency factor, or Oswald's efficiency factor, are unable to be properly expressed in analytical terms. Because the accuracy of these parameters is strongly sensitive to way the induced quantities are calculated, they are not entitled for numerical comparison.

4. Results and discussions

In this section the numerical results obtained with both models are compared to each other, and the accuracy of the numerical implementation is assessed by comparison with classical results. In all the following cases, $\lambda = c_t/c_r$ is the taper ratio (tip chord / root chord), Λ is the aspect ratio (b^2 / S), $\Lambda_{1/4}$ is the sweepback angle measured from the one-quarter-chord-line to the y-axis (spanwise direction), and φ is the spanwise twist distribution (degrees) and α is the angle of attack (degrees). The label " Far field drag in Trefftz Plane" refers to an idealization of the flow due to the fact that the downwash induced by the wake does not have an exact position determined on the wing. A single bound vortex line is assumed and the induced quantities are computed there. But, the fact is that a real wing does not have a single bound vortex and the velocity field induced by the wake varies along the chord. In order to obtain more accurate solutions, the flow is formulated in a plane far downstream, the so called Trefftz Plane, in terms of complex potential velocity, and a relationship between the flow in the Trefftz plane and the circulation $\Gamma(y)$ on the wing is then established. Such a connection is supported by the Helmboltz ´ s vortex theorem. A detailed description of the Trefftz´ s method can be found in Karamchetti (1966), and related issues are also treated by Smith (1995).

The first comparison is addressed to the lift slope (radian $^{-1}$) vs. aspect ratio as shown in Fig (5), from which it can be seen that the extended model yields lower values of lift, if compared to those yielded by the classical model. This is confirmed by Truckenbrodt (1979). A comparison is also made with results from the Trefftz Plane model as shown in Fig. (6), which reveals an excellent agreement.

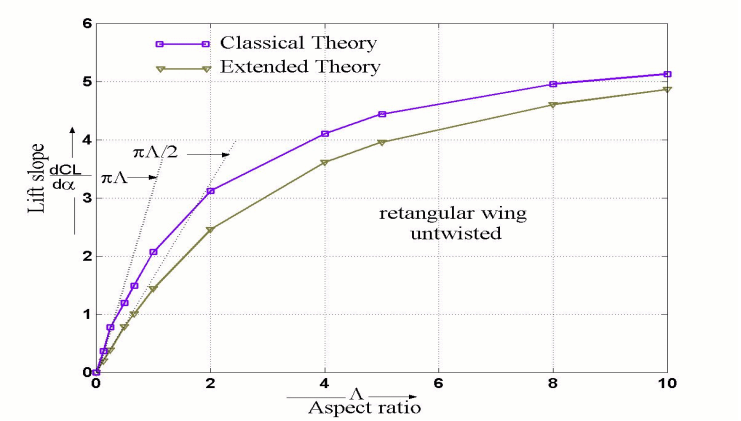

Figure 5. Lift Slope – Comparison between the classical and extended theories

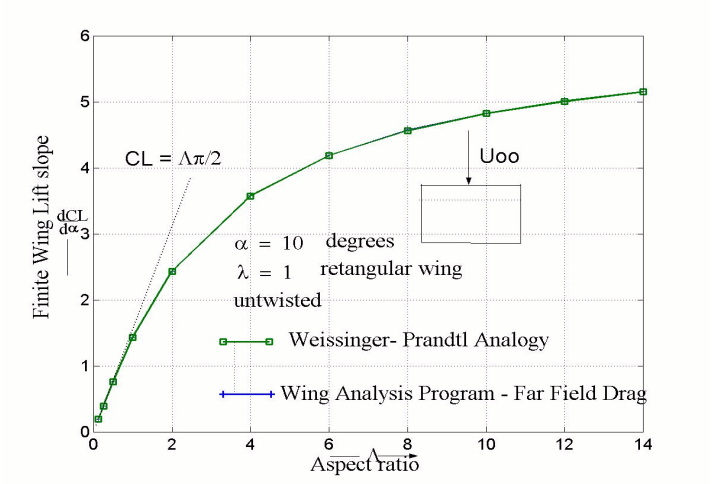

Figure 6. Lift Slope – Comparison between the extended model and a Trefttz-Plane-based variant

The formulation in the Trefftz Plane is described in detail by Karamchetti (1966), and further related topics can also be found in Smith (1995). The comparative analysis is now shifted to spanwise dimensionless distribution of circulation (or local lift scaled by the factor ρU_∞) as shown in Fig. (7), where lower values of lift yielded by extended model can be observed. Also comparatively lower values of vortex strenght (slope of the circulation distribution curve) for the extended model are noticeable, especially close to the wing tips.

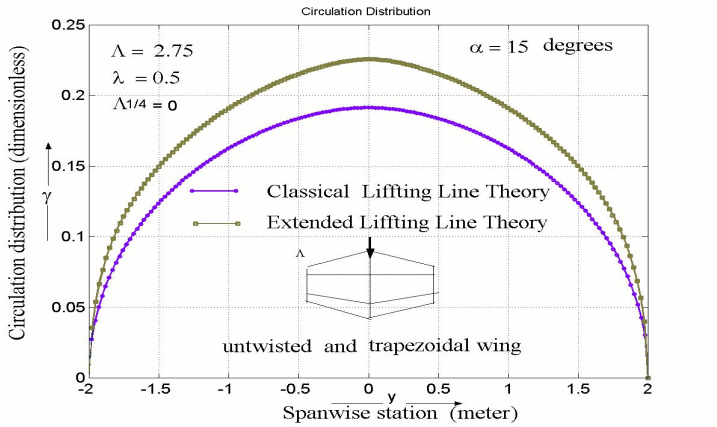

Figure 7. Spanwise Distribution of Circulation - Comparison Between the Classical and Extended Theories

Figure (8) reveals that the values for the wing lift coefficient obtained from Weissinger's model and those from the Trefttz Plane formulation (plotted against the spanwise twist ratio) are very close. Figure (8) also show that the values obtained from the extended theory is more conservative than the values form the classical theory.

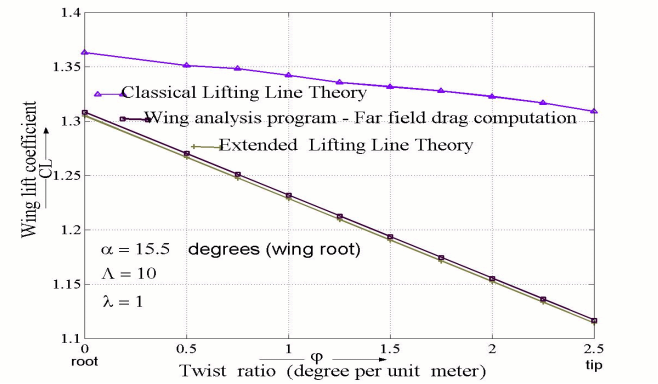

Figure 8. Wing lift coefficient – Comparison between the extended model and aTrefttz -Plane-based variant

The results presented in the preceding Figures are only concerned with symmetrical wing sections. However, wings with cambered sections can also be compared by means of the classical and extended models. Consider, for example, a finite wing with no aerodynamic twist and no geometric twist, having biconvex-parabolic-shaped sections described by the equation

$$Z = 2\,\frac{h}{c}\;X\,(1-X) \quad ; \quad Z = \frac{z}{c} \quad ; \quad X = \frac{x}{c} \tag{43}$$

where h is maximum value of the camber function. From the thin airfoil theory (Karamchetti, 1966) and the Pistolesi´ s Theorem, stated in Eq. (7), it is possible to show that.

$$\alpha_{L=0} = \left.\frac{dz}{dx}\right|_{x=3/4c} = -2\frac{h}{c} \tag{44}$$

Since the lift slope of the airfoil is not affected by the camber, again, one concludes that the extended model yields lower values of lift coefficient, for any angle of attack in the range $\alpha_{L=0} \le \alpha \le \alpha_{max}$, for a given aspect ratio, (see Fig. (5)), where the upper limit α_{max} is a parameter not predictable by the potential flow theory. In order to strengthen the accuracy of the numerical code implemented for the extended model, Fig (9) shows values of the induced drag coefficient resulting from both this model and Trefftz-Plane-based variant, for low and high aspect ratio limits, that agree very well**.**

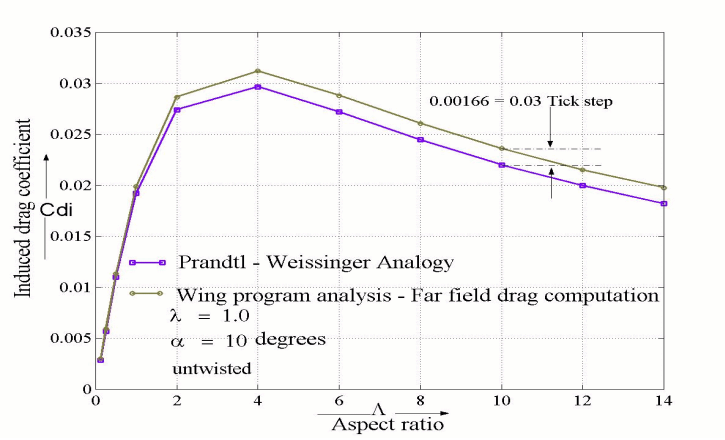

Figure 9. Wing induced drag coefficient, comparison between the extended model and a Trefftz-Plane-based variant.

It is worth emphasizing that the results presented so far are at the frontier of Classical Lifting Line-Theory in predicting non-viscous parameters for unswept wings with straight planform (rectangular and trapezoidal), twisted and possibly with cambered sections, whose simulation is absolutely viable through the extended model. The analysis is now addressed to sweptback wings, unable to be predicted by the classical model. The most suitable quantity entitled to strengthen the difference is the pitching moment that arises from the back shifting of the lifting-line. Figure. (10) shows the pitching moment coefficient C_{my} measured about the root quarter chord point vs. the spanwise twist distribution.

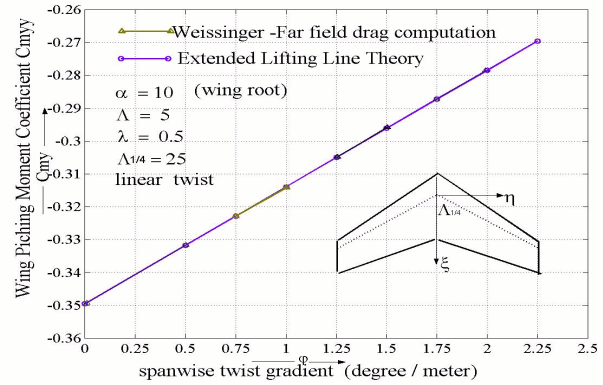

Figure 10. Wing pitching moment coefficient vs. spanwise twist - Extended model and Trefftz-Plane-based variant

It can be seen that the tendency to pitch the wing is decreased by the twist effect, that is, the aerodynamic load is relieved from the midsection to tip. Since *Cmy* is not an induced quantity, it is clear from Fig. (10) that extremely well matched results from the extended model and the Trefftz-Plane-based variant were achieved for a sweeping back angle of 25°. Next, Fig. (11) shows the combined effect of sweeping and geometric twist on the pitching moment coefficient. *Cmy*. The effects of sweeping and twist oppose each other.

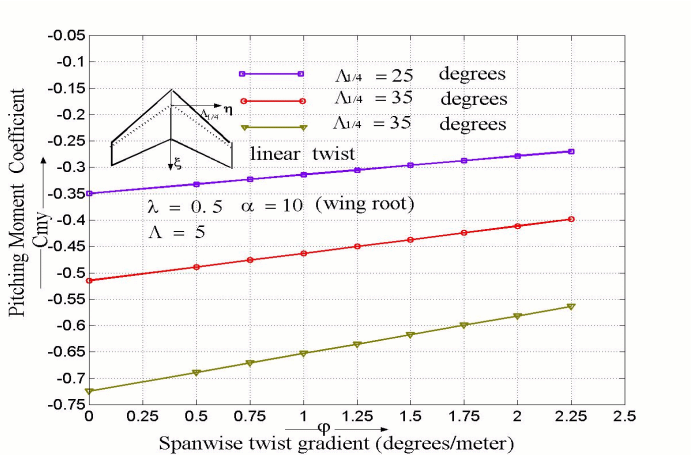

Figure 11. Wing pitching moment coefficient - combined effects of sweeping and twist by the extended model

5. Concluding Remarks.

A comparison between the Classical Lifting-Line Theory and the Extended Lifting Line Theory and its variants has been presented. This paper focused on the utilization, limitations, theoretical foundations and mostly, the extent of their applicability, ranging from the overlapping possibilities to the point where the extended model allows a step ahead. The results show that the extended model is a more powerful tool for preliminary wing design, allowing more aerodynamic parameters to be analyzed that the classical model. It is also made clear in this paper that, even though the present results are mainly concerned with low speed aerodynamics, some very meaningful insights are brought up in the field of high speed aerodynamics. An utterly convincing argument can be given when dealing with high speed airplane design. Sweeping wing is intended to reduce the compressibility effects, but, it is unavoidable to see that a twisted wing compensates for the tendency to nose down that results from the swept quarter-chord line. Such effects can be taken into account using the approach discussed in this paper. Finally, we strengthen that, among other contributions, the present work brings into evidence the parallelism between the analytical and numerical features of both theories, not easily found in the classical literature in such a clear way. Besides that, the innovative mathematical development performed in this work, from the extended model, allows for a term-by-term analogy that leads to a better comprehension of the relevant features and judgment of their potential as preliminary design tools.

6. References

Anderson, J.D,. Fundamentals of Aerodynamics, 2nd ed., Mc Graw- Hill, New York, 1991.

Bisplinghoff, R.L., Ashley, H., and Halfman. R.L., Aeroelasticity, Addison-Wesley, MA,1955, pp. 229-238.

Glauert, H., The Elements of Aerofoil and Airscrew Theory,2nd ed., Cambribge Univ. Press, Cambridge, England, UK, 1959

Karamchetti,K,. Principles of Ideal Fluid Aerodynamics , Wiley, New York, 1966, Chap. 19.

Rasmussen, M. L., and Smith, D.E., "Lifting-Line Theory for Arbitrarily Shaped Wings", Journal of Aircraft, Vol. 36, No.2, 1999, pp 340-347.

Robinson, A., and Laurmann, J. A., Wing Theory, Cambridge Univ. Press, Oxford, England, UK, 1956. Chap. 3.

Schlichting, H., and Truckenbrodt, E., Aerodynamics of the Airplane, McGraw-Hill, New York, 1979, Chap. 3.

Smith, S.C., "A Computational and Experimental Study of Non Linear Aspects of Induced Drag", Ph.D. Dissertation, Department of Aeronautics and Astronautics, Stanford University, CA, June, 1995, Chap. 3.

Thwaites, B., Incompressible Aerodynamics, Oxford Univ. Press, Oxford , England, UK, 1960.